ACES Asian Chemical Editorial Society

doi.org/10.1002/asia.202401498

CHEMISTRY AN ASIAN JOURNAL
Research Article

www.chemasianj.org

Stabilizing Contorted Doubly-Reduced Tetraphenylene with Heavy Alkali Metal Complexation: Crystallographic and Theoretical Evidence

Yikun Zhu,[a] Zheng Zhou,[a, b] Zheng Wei,[a] Alexandra Tsybizova,[c] Renana Gershoni-Poranne,*[d] and Marina A. Petrukhina*[a]

The two-fold reduction of tetrabenzo[*a*,*c*,*e*,*g*]cyclooctatetraene (TBCOT, or tetraphenylene, **1**) with K, Rb, and Cs metals reveals a distinctive core transformation pathway: a newly formed C–C bond converts the central eight-membered ring into a twisted core with two fused five-membered rings. This C–C bond of 1.589(3)–1.606(6) Å falls into a single σ-bond range and generates two perpendicular π-surfaces with dihedral angles of 110.3(9)°–117.4(1)° in the $\mathbf{1}_{TR}^{2-}$ dianions. As a result, the highly contorted $\mathbf{1}_{TR}^{2-}$ ligand exhibits a "butterfly" shape and could provide different coordination sites for metal-ion binding. The K-induced reduction of **1** in THF affords a polymeric product with low solubility, namely $[\{K^+(THF)\}_2(\mathbf{1}_{TR}^{2-})]$ ($\mathbf{K_2}$-$\mathbf{1}_{TR}^{2-}$). The use of a secondary ligand facilitates the isolation of discrete complexes with heavy alkali metals, $[Rb^+(18\text{-crown-6})]_2[\mathbf{1}_{TR}^{2-}]$ ($\mathbf{Rb_2}$-$\mathbf{1}_{TR}^{2-}$) and $[Cs^+(18\text{-crown-6})]_2[\mathbf{1}_{TR}^{2-}]$ ($\mathbf{Cs_2}$-$\mathbf{1}_{TR}^{2-}$). Both internal and external coordination are observed in $\mathbf{K_2}$-$\mathbf{1}_{TR}^{2-}$, while the bulky 18-crown-6 ligand only allows external metal binding in $\mathbf{Rb_2}$-$\mathbf{1}_{TR}^{2-}$ and $\mathbf{Cs_2}$-$\mathbf{1}_{TR}^{2-}$. The reversibility of the two-fold reduction and bond rearrangement is demonstrated by NMR spectroscopy. Computational analysis shows that the heavier alkali metals enable effective charge transfer from the $\mathbf{1}_{TR}^{2-}$TBCOT dianion, however, the aromaticity of the polycyclic ligand remains largely unaffected.

Introduction

Cyclooctatetraene (COT, C_8H_8, Scheme 1a), with its unique tub-shaped structure and variable coordination behavior, has been widely explored in reactions with different reducing agents, transition metals, and rare earth elements, resulting in a very extensive coordination chemistry.[1–5] The parent COT, as well as different COT-based derivatives, have been also utilized in different fields, including synthetic chemistry, magnetism, optical and electrical materials, biological and environmental applications.[6–13] The injection of two electrons into the COT core provides the most representative example of the reduction-induced aromatization accompanied by core planarization in COT^{2-}.[1,14,15] The resulting planar octagon exhibits η^8-coordination with multiple *d*- and *f*-elements and forms a great variety of organometallic compounds with different structures and compositions.[16–21]

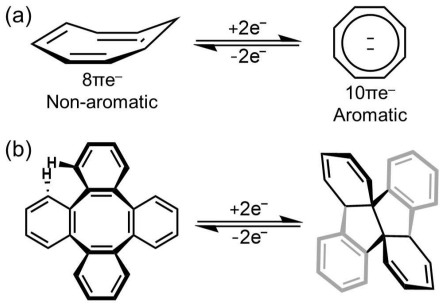

Scheme 1. Two-fold reduction of (a) COT and (b) TBCOT (**1**).

On the other hand, the π-extended COT derivative tetrabenzo[*a*,*c*,*e*,*g*]cyclooctatetraene (TBCOT, **1**, $C_{24}H_{16}$, Scheme 1b) is not able to adapt the same core planarization pathway. The steric repulsion between the hydrogen atoms at the *ortho*-positions reduces stability of the planar conformation and prevents the formation of the planarized central eight-membered ring. This was first illustrated by *in situ* NMR investigation back in 1981,[22] but only recently it was crystallographically confirmed upon chemical reduction of **1**.[23] Specifically, the stepwise reaction of **1** with Na metal in the presence of secondary ligand 18-crown-6 afforded the radical monoanion and dianion isolated with solvent-separated Na^+ counterions as single crystalline materials.[23] The X-ray diffraction analysis revealed that one electron injection reduces the core symmetry but allows the central eight-membered ring to keep a twisted tub structure. In contrast, the addition of the second electron

[a] *Y. Zhu, Z. Zhou, Z. Wei, M. A. Petrukhina*
Department of Chemistry, University at Albany, State University of New York, Albany, NY 12222, USA
E-mail: mpetrukhina@albany.edu

[b] *Z. Zhou*
School of Materials Science and Engineering, Tongji University, Shanghai 201804, China

[c] *A. Tsybizova*
Laboratory for Organic Chemistry, ETH Zürich, Vladimir-Prelog-Weg 2, Zürich 8092, Switzerland

[d] *R. Gershoni-Poranne*
Schulich Faculty of Chemistry, Resnick Sustainability Center for Catalysis, Technion – Israel Institute of Technology, Technion City 32000, Israel
E-mail: rporanne@technion.ac.il

Supporting information for this article is available on the WWW under https://doi.org/10.1002/asia.202401498

leads to a distinctive core transformation: a new C–C single bond is formed, converting the eight-membered ring into two fused five-membered rings in $\mathbf{1}_{TR}^{2-}$ (Scheme 1b).

In $\mathbf{1}_{TR}^{2-}$, the formation of the new C–C single bond generates two π-surfaces (*i.e.*, the two halves of the molecule) oriented nearly perpendicular (111°) to each other (Scheme 2). This configuration of the dianion creates internal and external surfaces that can serve as potential sites for metal coordination. Despite these original binding abilities, to date, only solvent-separated ion-products (SSIPs) have been isolated for TBCOT and its derivatives.[23,24]

Compared to alkali metals with smaller ionic radii, Li^+ and Na^+, which favor the formation of SSIPs with a variety of π-ligands,[25–27] the heavier alkali metals, K^+, Rb^+, and Cs^+, tend to complex with the carbanions through direct metal ion coordination.[28–30] Particularly, the large size of Cs^+ ion and enhanced metal-π interactions favour the selective concave binding to various curved π-hosts, including several carbon bowls and nanographenes.[31–37]

In this work, we investigate the chemical reduction behavior of TBCOT with heavy alkali metals and focus on metal coordination effects. We target the isolation of single crystals of the contact-ion products (CIPs) and their characterization with X-ray diffraction and spectroscopic methods. The insights into the effect of heavy alkali metal ion binding are sought with the help of theoretical methods.

Results and Discussion

Chemical Reduction and X-Ray Diffraction Characterization

To enhance the cation-anion interactions and investigate the effect of metal binding, we selected three alkali metals, K, Rb, and Cs (Scheme 2). The K-induced reaction of **1** in THF readily produced the single crystalline product in *ca.* 53% yield. Its X-ray crystallographic characterization revealed the formation of an organometallic polymer, namely $[\{K^+(THF)\}_2(\mathbf{1}_{TR}^{2-})]\cdot 0.5\ C_6H_{14}$ ($\mathbf{K_2\text{-}1}_{TR}^{2-}\cdot 0.5\ C_6H_{14}$). In contrast, the solubility of the corresponding products stemming from the Rb- and Cs-based reactions in THF was very limited. Consequently, the secondary ligand, 18-crown-6 ether, was used to increase the solubility and to facilitate the product crystallization. Under similar conditions, two discrete CIPs were isolated with Rb^+ and Cs^+ counterions, namely $[M^+(18\text{-crown-}6)]_2[\mathbf{1}_{TR}^{2-}]$·(M=Rb or Cs). These complexes were crystallized with different interstitial solvent molecules as $\mathbf{Rb_2\text{-}1}_{TR}^{2-}\cdot 1.88THF\cdot 0.06\ C_6H_{14}$ and $\mathbf{Cs_2\text{-}1}_{TR}^{2-}\cdot 3.5THF$. The formation of a new C–C bond is observed in all the reduced products, breaking the π-conjugation inside the six-membered ring A and C, but leaving the other two benzene rings B and D less disturbed (Scheme 2).

In contrast to the previously reported solvent-separated sodium(I) products,[23] the lack of secondary ligand, 18-crown-6, allows multiple direct K–C interactions from both internal and external sides of $\mathbf{1}_{TR}^{2-}$ (Figure 1b). In the crystal structure of $\mathbf{K_2\text{-}1}_{TR}^{2-}$ (Figure 1a), there are two crystallographically independent K^+ ions with different coordination environments. K1 is internally sandwiched by two six-membered rings B and D of one $\mathbf{1}_{TR}^{2-}$ anion in an asymmetric η^6-fashion (3.08(3)–3.56(3) Å).

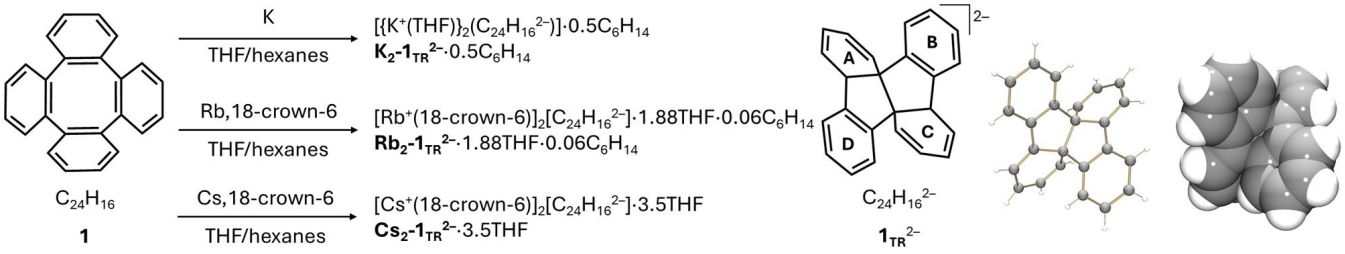

Scheme 2. Chemical reduction of **1** with heavy alkali metals, along with the crystal structure of the dianion $\mathbf{1}_{TR}^{2-}$, ball-and-stick and space-filling models.

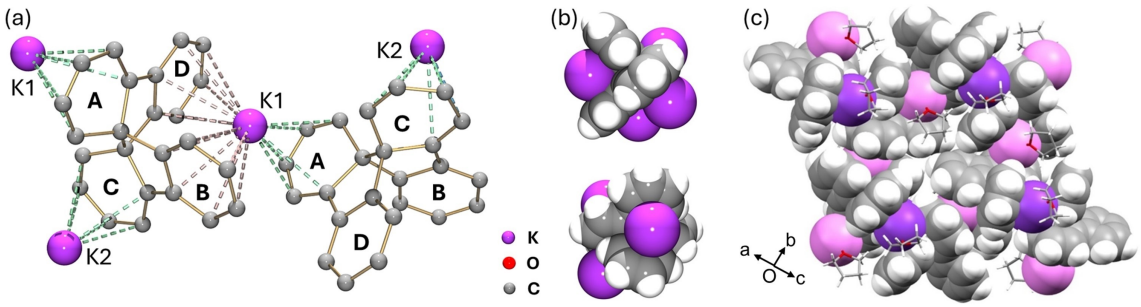

Figure 1. (a) Crystal structure of $\mathbf{K_2\text{-}1}_{TR}^{2-}$, ball-and-stick model. The THF molecules and hydrogen atoms are omitted for clarity. The external contacts are shown as green dashes. (b) Metal coordination pattern of $\mathbf{1}_{TR}^{2-}$ in different views, space-filling model. (c) 2D layer of $\mathbf{K_2\text{-}1}_{TR}^{2-}$, mixed model. Two independent K^+ ions are shown in different shades of purple.

Through the remaining open site, this K1 ion externally coordinates to the six-membered ring A of the second $\mathbf{1}_{TR}^{2-}$ anion in the η^5-fashion (K–C: 2.96(2)–3.31(5) Å) and to one THF molecule. K2 also has one coordinated THF molecule and exhibits η^5-coordination to ring C (3.02(2)–3.16(2) Å) from the external side of $\mathbf{1}_{TR}^{2-}$. Furthermore, multiple additional K–C interactions (2.86(3)–3.46(4) Å, Table S5) with the third $\mathbf{1}_{TR}^{2-}$ anion expand the organometallic framework into a 2D layer (Figures 1c and S18).

To break the polymeric motif and to investigate the preferred coordination sites of $\mathbf{1}_{TR}^{2-}$, the secondary ligand, 18-crown-6 ether, was introduced in the reduction reactions with Rb or Cs metals. Unlike Na metal,[23] the Rb^+ and Cs^+ ions tend to directly coordinate to the negatively charged π-surface, even in the presence of secondary ligands.[38–41] In both crystal structures of $\mathbf{Rb_2\text{-}1}_{TR}^{2-}$ and $\mathbf{Cs_2\text{-}1}_{TR}^{2-}$ (Figure 2), the two cations are asymmetrically η^5-coordinated (Figure 2cd, see Table S6 for more details) to the opposite external six-membered rings A and C of $\mathbf{1}_{TR}^{2-}$, in a similar manner as in $\mathbf{K_2\text{-}1}_{TR}^{2-}$. The coordination environment of each Rb^+/Cs^+ ion is completed by 18-crown-6 ether ($Rb–O_{crown}$: 2.861(2)–3.135(2) Å; $Cs–O_{crown}$: 2.989(3)–3.256(3) Å). The larger radius of the Cs^+ ion enables its additional coordination to the adjacent benzene ring (Figure 2b, Cs1–C3: 3.466(4) Å and Cs2–C7: 3.697(4) Å), thus moving the Cs^+ ions closer to the bridging C2–C3 and C6–C7 sites (Table S6). All M–C and M–O (M=Rb and Cs) distances are close to the previously reported values.[28–32]

In the solid-state structure of $\mathbf{Rb_2\text{-}1}_{TR}^{2-}$, additional C–H···π interactions (2.500(3)–2.624(3) Å) between the neighbouring 18-crown-6 ether moieties and the $\mathbf{1}_{TR}^{2-}$ anions result in the formation of zig-zag columns (Figure 2d). The solid-state structure of $\mathbf{Cs_2\text{-}1}_{TR}^{2-}$ also exhibits 1D column packing, but it forms a linear column instead, held by C–H···π interactions (2.541(5)/2.703(5) Å) between the anions and adjacent cationic moieties. Additionally, a 3_1 screw axis in the 1D column of $\mathbf{Cs_2\text{-}1}_{TR}^{2-}$ segments the column into $[\mathbf{Cs_2\text{-}1}_{TR}^{2-}]_3$ molecular units (Figure 2e).

In all $\mathbf{1}_{TR}^{2-}$ anions, the two-electron addition enforces the transformation of the central eight-membered ring into a bicyclic core through the formation of a new C–C bond ***a*** between the C1 and C5 atoms. This bond measures 1.605(6) Å in $\mathbf{Na_2\text{-}1}_{TR}^{2-}$,[23] 1.60(3) Å in $\mathbf{K_2\text{-}1}_{TR}^{2-}$, 1.589(3) Å in $\mathbf{Rb_2\text{-}1}_{TR}^{2-}$, and 1.606(6) Å in $\mathbf{Cs_2\text{-}1}_{TR}^{2-}$. All bond lengths are considerably longer than the reported value of 1.560(10) Å in the OMT^{2+} cation,[42] but fall into a narrower range compared to the octaphenyl-substituted TBCOT (1.545(9)/1.619(11) Å).[24] Consequently, the C–C bonds around the C1 and C5 centers are elongated to the typical C–C single bond range, breaking the π-electron delocalization through the six-membered rings A and C. Except for the single bonds ***b*** and ***c***, only bond ***e*** is significantly shortened to the double bond range (highlighted in red in Table 1). The remaining C–C bonds ***f***, ***g***, and ***h***, along with the bridging bond ***i***, stay within the typical aromatic bond range (Table 1), indicating possible π-conjugation to the benzene ring D. Notably, within the formally aromatic benzene rings B and D, an increased bond length alternation (BLA, Table S2) is observed, suggesting the aromaticity reduction compared to neutral **1**.

The structurally characterized π-complexes offer valuable experimental benchmarks for evaluation of metal binding influence on the $\mathbf{1}_{TR}^{2-}$ core. The dihedral angles between the

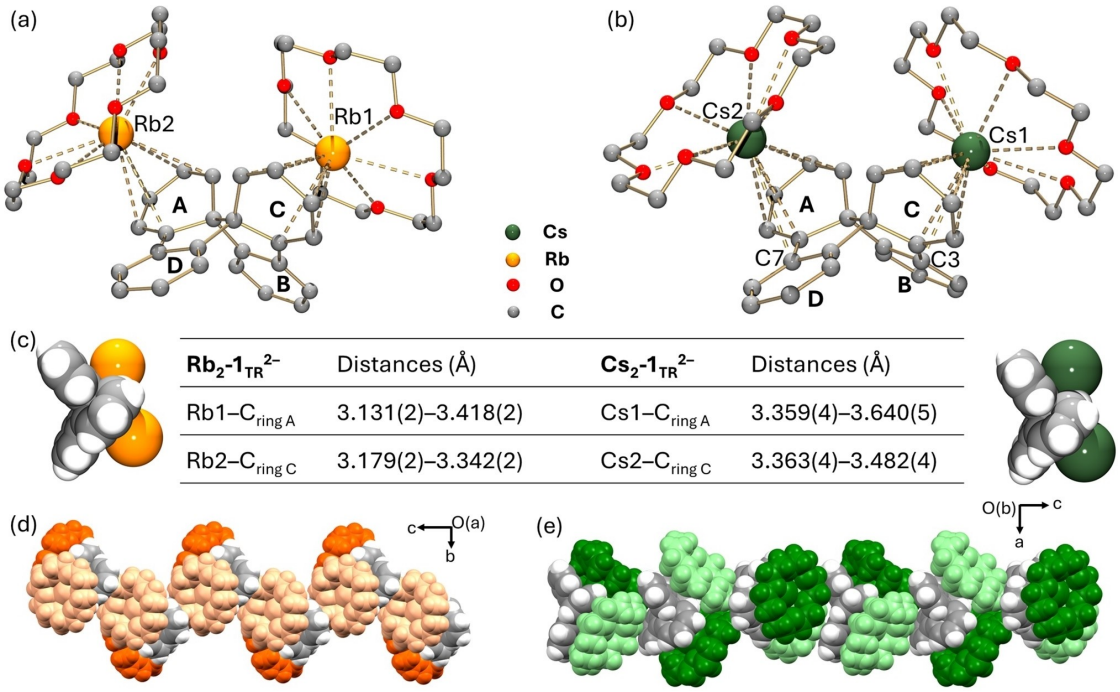

$\mathbf{Rb_2\text{-}1}_{TR}^{2-}$	Distances (Å)	$\mathbf{Cs_2\text{-}1}_{TR}^{2-}$	Distances (Å)
$Rb1–C_{ring\ A}$	3.131(2)–3.418(2)	$Cs1–C_{ring\ A}$	3.359(4)–3.640(5)
$Rb2–C_{ring\ C}$	3.179(2)–3.342(2)	$Cs2–C_{ring\ C}$	3.363(4)–3.482(4)

Figure 2. Crystal structures of (a) $\mathbf{Rb_2\text{-}1}_{TR}^{2-}$ and (b) $\mathbf{Cs_2\text{-}1}_{TR}^{2-}$, ball-and-stick models. All hydrogen atoms are omitted for clarity. (c) Metal coordination pattern of $\mathbf{1}_{TR}^{2-}$ in both compounds, along with the Rb–C and Cs–C distances, space-filling model. 1D column packing in (d) $\mathbf{Rb_2\text{-}1}_{TR}^{2-}$ and (e) $\mathbf{Cs_2\text{-}1}_{TR}^{2-}$, space-filling model. Independent Rb^+/Cs^+ ions are highlighted in different shades of orange/green.

Table 1. Selected average C–C bond distances (Å) and dihedral angles (°) in $\mathbf{1}_{TR}^{2-}$ anions, along with a labeling scheme.

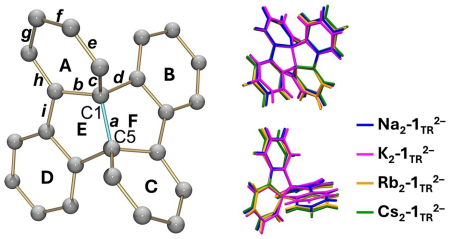

	Na_2-$\mathbf{1}_{TR}^{2-}$[23]	K_2-$\mathbf{1}_{TR}^{2-}$	Rb_2-$\mathbf{1}_{TR}^{2-}$	Cs_2-$\mathbf{1}_{TR}^{2-}$
a (C1–C5)	1.605(6)	1.60(3)	1.589(3)	1.606(6)
e	1.358(6)	1.36(2)	1.367(3)	1.363(6)
f	1.416(6)	1.47(1)	1.424(3)	1.428(7)
g	1.387(6)	1.41(2)	1.403(3)	1.400(7)
h	1.382(6)	1.37(2)	1.387(3)	1.394(6)
i	1.420(6)	1.44(2)	1.440(3)	1.429(6)
∠B/D	103.3(5)	92.0(9)	114.6(1)	121.2(1)
∠E/F	111.0(5)	110.3(9)	117.4(1)	117.4(1)
∠A/D (∠B/C)	20.6(5)	4.9(9)	19.6(1)	29.9(1)
∠A/E (∠C/F)	23.0(5)	14.9(9)	21.7(1)	27.4(1)
∠D/E (∠B/F)	4.0(5)	10.1(9)	4.0(1)	2.5(1)

two newly formed five-membered rings E and F are calculated to be 110.3(9)° in $\mathbf{K_2}$-$\mathbf{1}_{TR}^{2-}$, comparable to the value in $\mathbf{Na_2}$-$\mathbf{1}_{TR}^{2-}$ (111.0(5)°), but those are slightly larger in $\mathbf{Rb_2}$-$\mathbf{1}_{TR}^{2-}$ and $\mathbf{Cs_2}$-$\mathbf{1}_{TR}^{2-}$ (117.4(1)°), which may be a result of uneven heavy alkali metal ion coordination.

Although the K^+ coordination causes only minor influence on the five-membered rings of $\mathbf{1}_{TR}^{2-}$, the effect is more pronounced for the six-membered rings. The internal K^+ coordination drags the two involved benzene rings B and D towards the metal center, thereby largely reducing the dihedral angle ∠B/D (vs. ∠E/F) and increasing the ∠D/E angle. Instead of disturbing the planarity of aromatic rings B and D and further reducing their aromaticity, the metal binding reduces the planarity of the non-aromatic five-membered rings E and F (Table S7) to maximize the benefits from both aromaticity and metal coordination.

Effect of Metal Coordination on Stability

In addition to crystallographic data, the core transformation is confirmed by *in situ* NMR spectroscopy. Similar to $\mathbf{Na_2}$-$\mathbf{1}_{TR}^{2-}$,[23] the ^{1}H NMR spectrum of $\mathbf{K_2}$-$\mathbf{1}_{TR}^{2-}$ (Figure 3a) shows a clear symmetry reduction, successfully reproducing the data reported back in 1981[22] but with improved resolution. The ^{1}H NMR spectra of the Rb- and Cs-products have similar patterns (Figures S7 and S11) but with slightly different chemical shifts, as revealed by the correlated (^{1}H-^{1}H COSY) spectroscopy (Figures S9 and S13). The formation of sp^3-hybridized C-centers in $\mathbf{1}_{TR}^{2-}$ is also supported by the new ^{13}C NMR resonance observed at ~61 ppm for all three CIPs (See supporting information for more details).

In addition, the UV-vis spectroscopy investigation of all products reveals distinct solution colour and absorption pattern changes. In the Na-induced reduction, the reaction mixture displayed a colour change from colourless (neutral) to pale green (mono-reduced product) and darker green for the doubly-reduced product, with clear stepwise changes observed in the UV-vis absorption patterns.[23] In contrast, the addition of heavier K, Rb, or Cs metals to the initially colourless solution of **1**, regardless of the presence of 18-crown-6 ether, rapidly generated a stable dark purple colour persistent for 24 hours (Figure 3b), indicating the formation of the doubly-reduced products without showing an intermediate state (Figures S1–S3).

By controlling the reaction time (*ca.* 5 minutes), the "naked" radical anion can be isolated with Na^+ counterions, but in the case of Rb metal, the crystals of $\mathbf{Rb_2}$-$\mathbf{1}_{TR}^{2-}$ were isolated along with the crystals of neutral TBCOT (Figure S14). The observed difference points to potential stabilization of the doubly-reduced state over the intermediate monoanion by heavy alkali metal ion binding.

Computational Analysis

To understand the influence of metal coordination on the reduction process and the reduced products, DFT calculations were performed for the SSIPs and CIPs (see supporting information for more details). Due to the polymeric nature of $\mathbf{K_2}$-$\mathbf{1}_{TR}^{2-}$, it was omitted from this analysis.

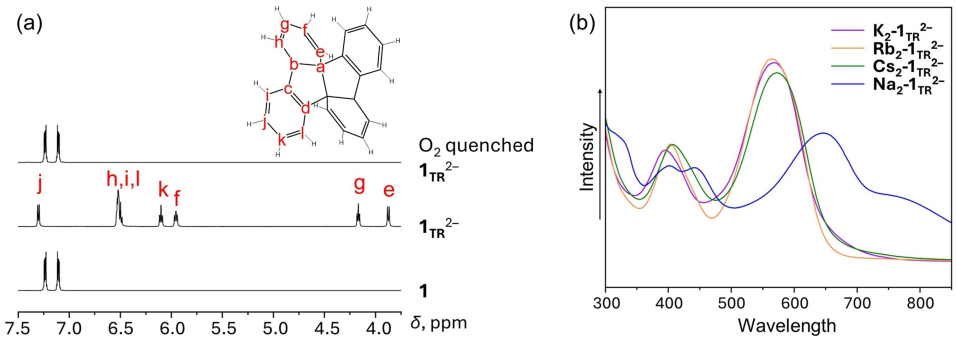

Figure 3. (a) ^{1}H NMR investigation of the two-fold reduction of TBCOT with K. (b) UV-vis absorption spectra of all products.

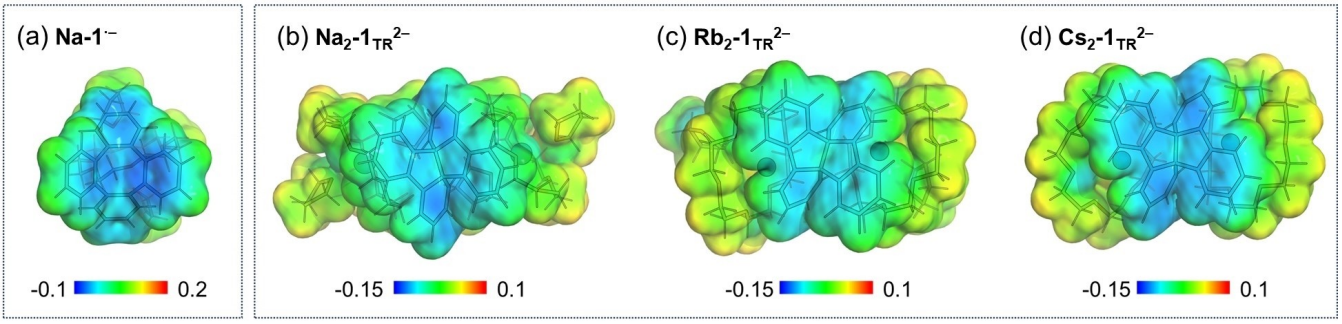

Figure 4. Electrostatic potential surfaces of (a) **Na-1**$^-$, (b) **Na$_2$-1$_{TR}^{2-}$**, (c) **Rb$_2$-1$_{TR}^{2-}$**, and (d) **Cs$_2$-1$_{TR}^{2-}$**.

The X-ray structure of ion-pair **Na-1**$^-$ shows a lack of direct metal ion coordination to the polycyclic aromatic core. Nevertheless, computations indicate that there are geometric and electronic consequences to the proximity of the sodium cation. The total charge on the monoanion is reduced from −1.00–−0.84, meaning that the anion relieves −0.16 charge (16%) via charge transfer to the neighboring cationic moiety.

Next, the effect of heavy alkali metal binding was evaluated by comparing the solvent-separated **Na$_2$-1$_{TR}^{2-}$** product to two π-complexes, **Rb$_2$-1$_{TR}^{2-}$** and **Cs$_2$-1$_{TR}^{2-}$**. The total charge on the **1$_{TR}^{2-}$** anion is −1.83, −1.17, and −1.26, corresponding to losses of 8%, 42%, and 37% for **Na$_2$-1$_{TR}^{2-}$**, **Rb$_2$-1$_{TR}^{2-}$**, and **Cs$_2$-1$_{TR}^{2-}$**, respectively (charge distributions are depicted visually in Figure 4). In the latter two cases, the dianion directly interacts with two metal centers, which explains the notably reduced charges. These values indicate that charge transfer from the polycyclic dianion to the metal is a mechanism for overall stabilization. Not surprisingly, the charge transfer is notably more efficient in the heavy alkali metal products, where there is direct metal complexation to the π-ligand, in contrast to the solvent-separated sodium(I) product. For Rb^+ and Cs^+, the large ionic size causes it to extend outward from the crown ether perimeter, which allows both to have better contact with the aromatic system. However, as observed from the crystal structure, the overall shorter Rb–C distances to the ligand core may explain the greater extent of charge transfer to this ion (Figure 2c).

Complexation also affects the newly formed C–C bond. The uncomplexed **1$_{TR}^{2-}$** displays a Mayer bond order of 1.11, which is indicative of a single bond. Although the value is greater than 1, this does not necessarily imply a strong bond. As demonstrated by Bridgeman et al.,[43] the Mayer bond order is highly method dependent. For example, the C–C single bond in ethane has values between 0.95–1.12. Non-integer values are common when large basis sets are employed and when complex systems are studied. Notably, interactions with the cationic moieties slightly increase this value to 1.27, 1.18, and 1.20, for Na, Rb, and Cs, respectively. This suggests that transferring charge to the metal(s) strengthens the new C–C bond, possibly by removing electron density from high-lying molecular orbitals with antibonding character. However, a quantitative correlation between the bond order and charge could not be found.

The **1$_{TR}^{2-}$** has two sets of identical six-membered rings – one set regains aromaticity after the cyclization (the rings denoted in pink in Figure 5a) and the other becomes non-aromatic due to the loss of full cyclic conjugation (the rings colored in blue in Figure 5a). For all three species, the aromatic "pink" rings display the smallest partial charges while most of the charge is delocalized on the non-aromatic "blue" components (pink: −0.27, −0.14, −0.16; blue: −0.66, −0.44, −0.46, for the Na^+, Rb^+, and Cs^+ products, respectively). The two heavier alkali metals have notably smaller partial charges, commensurate with the more efficient charge transfer observed in these cases.

Interestingly, despite the non-negligible difference in the partial charges between the three species, there is hardly any difference in the aromaticity evaluation. In all three cases, the NICS(1.7)$_{zz}$ values of the A rings are approximately −16 ppm and the HOMA values are above 0.9, indicating moderate-to-

(a)

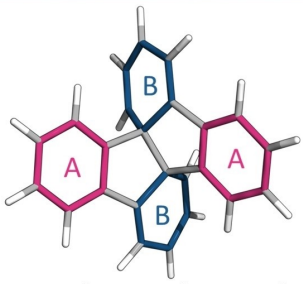

Na$_2$-1$_{TR}^{2-}$/ Rb$_2$-1$_{TR}^{2-}$/ Cs$_2$-1$_{TR}^{2-}$

(b)

Compound	Ring	Partial charge	*NICS*(1.7)$_{zz}$	HOMA
Na$_2$-1$_{TR}^{2-}$	*A*	–0.27	–16	0.91
	B	–0.66	–	–
Rb$_2$-1$_{TR}^{2-}$	*A*	–0.14	–17	0.94
	B	–0.44	–	–
Cs$_2$-1$_{TR}^{2-}$	*A*	–0.16	–16	0.90
	B	–0.46	–	–

Figure 5. (a) Schematic 3D structure of the aromatic component of the **Na$_2$-1$_{TR}^{2-}$**, **Rb$_2$-1$_{TR}^{2-}$**, and **Cs$_2$-1$_{TR}^{2-}$** products. The different sets of rings are color-coded identified by the letters A and B. (b) Partial charges and aromaticity (NICS in ppm and HOMA) metrics for the respective rings in the different species.

strong aromaticity in the A rings. For comparison, the uncomplexed $\mathbf{1}_{TR}^{2-}$ has NICS(1.7)$_{zz}$ = −13 ppm and HOMA = 0.93.[23] Altogether, these results suggest that the cyclized structure is stabilized by the aromaticity in the A rings, and this stabilization is largely unaffected by the charge transfer that is achieved by complexation of alkali metals.

Conclusions

In this work, the chemical reduction of TBCOT (**1**) was investigated with heavy alkali metals, K, Rb, and Cs, with/without the presence of a secondary ligand. Several doubly-reduced products were isolated in the complexed form and fully characterized by X-ray crystallographic and spectroscopic methods. All doubly-reduced anions exhibit the distinctive reduction-induced core transformation from the tub-shaped eight-membered ring to a twisted structure with two fused five-membered rings, as in the "naked" form of $\mathbf{1}_{TR}^{2-}$. The isolation of several doubly-reduced products with different alkali metals allowed the evaluation of the metal binding preferences and negative charge distribution, illustrating sufficient flexibility of the contorted bicyclic core. Notably, all these transformations are fully reversible, and the detected charge-dependent core rearrangement of TBCOT could enable potential applications as redox active molecular switches. Comprehensive computational analysis was used to further characterize the reduction products, as well as to elucidate the changes in aromaticity, charge delocalization patterns, and the effect of metal complexation coupled with reduction. Importantly, a notable difference in charge transfer (8% *vs. ca.* 40%) between a solvent-separated ion product and complexed products was revealed computationally. These results provide new insights which should advance organometallic chemistry of heavy alkali metals with contorted π-ligands.

Experimental Section

Materials and Methods

All manipulations were carried out using break-and-seal and glovebox techniques under an atmosphere of argon (Airgas, UHP grade 99.999%).[44,45] Tetrahydrofuran (THF) and hexanes (Sigma Aldrich) were dried over Na/benzophenone and distilled prior to use. Tetrahydrofuran-d_8 (≥99.5 atom %D, Sigma Aldrich) was dried over NaK_2 alloy and vacuum-transferred. Potassium (98%), rubidium (99.5%), cesium (99.5%), and 18-crown-6 ether (99%) were purchased from Sigma Aldrich and used as received. TBCOT ($C_{24}H_{16}$, **1**) was synthesized and purified according to the previously reported method.[23] The UV-vis absorption spectra were recorded on a Shimadzu UV-2600i UV-vis spectrophotometer. The ^{1}H, ^{13}C, ^{1}H-^{1}H COSY, and ^{1}H-^{13}C HSQC NMR spectra were recorded on a Bruker Ascend-500 spectrometer. Chemical shifts (δ) are reported in parts per million (ppm) and referenced to the resonances of the corresponding solvent used. The extreme oxygen- and moisture sensitivity of the reduced products, $\mathbf{K_2}$-$\mathbf{1}_{TR}^{2-}$ to $\mathbf{Cs_2}$-$\mathbf{1}_{TR}^{2-}$, along with the presence of interstitial hexane and THF molecules, prevented obtaining elemental analysis data. The crystal structure description and refinement details[44] are reported in the supporting information.

[{K$^+$(THF)}$_2$($C_{24}H_{16}^{2-}$)]·0.5 C_6H_{14} (K_2-$\mathbf{1}_{TR}^{2-}$·0.5 C_6H_{14})

THF (1.5 mL) was added to a customized glass system containing excess K metal (3.0 mg, 0.0769 mmol) and **1** (2.0 mg, 0.0066 mmol). The reaction mixture was stirred at 25 °C under argon for 20 hours. The initial off-white colour (neutral ligand) changed to purple in 25 minutes and remained the same until the reaction was stopped. The mixture was filtered after 20 hours, and the purple filtrate was layered with 1.0 mL of anhydrous hexanes. The ampule was sealed under argon and stored at 5 °C. After 7 days, block-shaped crystals formed in the ampule. Yield: 5 mg, 53%. UV-vis (THF, λ_{max}, nm): 300(sh), 394, 567. ^{1}H NMR (THF-d_8, ppm, 25 °C): δ = 3.86–3.87 (2H, $\mathbf{1}_{TR}^{2-}$), 4.15–4.17 (2H, $\mathbf{1}_{TR}^{2-}$), 5.93–5.96 (2H, $\mathbf{1}_{TR}^{2-}$), 6.08–6.11 (2H, $\mathbf{1}_{TR}^{2-}$), 6.48–6.54 (6H, $\mathbf{1}_{TR}^{2-}$), 7.29–7.31 (2H, $\mathbf{1}_{TR}^{2-}$). ^{13}C NMR (THF-d_8, ppm, 25 °C): δ = 61.72, 86.36, 95.86, 101.76, 113.91, 117.92, 120.25, 126.86, 127.18, 128.73, 142.78, 155.37.

[Rb$^+$(18-crown-6)]$_2$[$C_{24}H_{16}^{2-}$]·1.88THF·0.06 C_6H_{14} (Rb_2-$\mathbf{1}_{TR}^{2-}$·1.88THF·0.06 C_6H_{14})

THF (1.5 mL) was added to a customized glass system containing excess Rb metal (4.0 mg, 0.0467 mmol), 18-crown-6 ether (3.5 mg, 0.0132 mmol), and **1** (2.0 mg, 0.0066 mmol). The reaction mixture was stirred at 25 °C under argon for 20 hours. The initial off-white color (neutral ligand) changed to purple in 15 minutes and remained the same until the reaction was stopped. The mixture was filtered after 20 hours, and the purple filtrate was layered with 1.0 mL of anhydrous hexanes. The ampule was sealed under argon and stored at 5 °C. After 7 days, block-shaped crystals formed in the ampule. Yield: 3.0 mg, 40%. UV-vis (THF, λ_{max}, nm): 300(sh), 404, 565. ^{1}H NMR (THF-d_8, ppm, 25 °C): δ = 4.17–4.19 (2H, $\mathbf{1}_{TR}^{2-}$), 4.21–4.23 (2H, $\mathbf{1}_{TR}^{2-}$), 5.88–5.91 (2H, $\mathbf{1}_{TR}^{2-}$), 6.03–6.06 (2H, $\mathbf{1}_{TR}^{2-}$), 6.40–6.43 (2H, $\mathbf{1}_{TR}^{2-}$), 6.49–6.52 (4H, $\mathbf{1}_{TR}^{2-}$), 7.38–7.40 (2H, $\mathbf{1}_{TR}^{2-}$). ^{13}C NMR (THF-d_8, ppm, 25 °C): δ = 61.06, 86.22, 96.45, 102.04, 114.97, 117.50, 119.79, 126.38, 126.40, 128.55, 143.30, 156.92.

[Cs$^+$(18-crown-6)]$_2$[$C_{24}H_{16}^{2-}$]·3.5THF (Cs_2-$\mathbf{1}_{TR}^{2-}$·3.5THF)

THF (1.5 mL) was added to a customized glass system containing excess Cs metal (2.0 mg, 0.0150 mmol), 18-crown-6 ether (8.0 mg, 0.0303 mmol), and **1** (2.0 mg, 0.0066 mmol). The reaction mixture was stirred at 25 °C under argon for 20 minutes. The initial off-white color (neutral ligand) changed to purple with a large amount of precipitate in 5 minutes and remained the same until the reaction was stopped. The mixture was filtered after 20 minutes, and the purple filtrate was layered with 0.5 mL of anhydrous hexanes. The ampule was sealed under argon and stored at 5 °C. After 4 days, needle-shaped crystals formed in the ampule. Yield: 2.0 mg, 23%. UV-vis (THF, λ_{max}, nm): 300(sh), 408, 574. ^{1}H NMR (THF-d_8, ppm, 25 °C): δ = 4.02–4.04 (2H, $\mathbf{1}_{TR}^{2-}$), 4.32–4.35 (2H, $\mathbf{1}_{TR}^{2-}$), 5.81–5.84 (2H, $\mathbf{1}_{TR}^{2-}$), 6.06–6.09 (2H, $\mathbf{1}_{TR}^{2-}$), 6.39–6.41 (2H, $\mathbf{1}_{TR}^{2-}$), 6.44–6.50 (4H, $\mathbf{1}_{TR}^{2-}$), 7.29–7.31 (2H, $\mathbf{1}_{TR}^{2-}$). ^{13}C NMR (THF-d_8, ppm, 25 °C): δ = 60.52, 86.31, 96.14, 101.44, 113.91, 116.83, 120.75, 125.84, 126.26, 128.26, 143.66, 156.03.

Acknowledgements

Financial support of this work from the U. S. National Science Foundation, CHE-2404031, is acknowledged by M. A. P. NSF's ChemMatCARS Sector 15 is principally supported by the

Divisions of Chemistry (CHE) and Materials Research (DMR), National Science Foundation, under grant number NSF-CHE-1834750. The use of the Advanced Photon Source, an Office of Science User Facility operated for the U.S. Department of Energy (DOE) Office of Science by Argonne National Laboratory, was supported by the U.S. DOE under Contract No. DE-AC02-06CH11357. A. T. and R. G. P. express their gratitude for the support of Prof. Dr. Peter Chen (ETH Zürich). R. G. P. is a Branco Weiss Fellow and Horev Fellow.

Conflict of Interests

The authors declare no conflict of interest.

Data Availability Statement

The data that support the findings of this study are provided in the ESI. Deposition numbers 2389784 (for Rb$\mathbf{K_2}$-$\mathbf{1}_{TR}^{2-}$), 2389785 (for K$\mathbf{Rb_2}$-$\mathbf{1}_{TR}^{2-}$), and 2389786 (for $\mathbf{Cs_2}$-$\mathbf{1}_{TR}^{2-}$) contain the supplementary crystallographic data for this paper. These data are provided free of charge by the joint Cambridge Crystallographic Data Centre and Fachinformationszentrum Karlsruhe Access Structures service.

Keywords: Chemical reduction · Tetrabenzocyclooctatetraene · Alkali metal coordination · DFT · Aromaticity

[1] T. J. Katz, *J. Am. Chem. Soc.* **1960**, *82*, 3784–3785.
[2] T. J. Katz, *J. Am. Chem. Soc.* **1960**, *82*, 3785–3786.
[3] A. Avdeef, K. N. Raymond, K. O. Hodgson, A. Zalkin, *Inorg. Chem.* **1972**, *11*, 1083–1088.
[4] V. Lavallo, R. H. Grubbs, *Science* **2009**, *326*, 559–562.
[5] A. Jr. Streitwieser, U. Mueller-Westerhoff, *J. Am. Chem. Soc.* **1968**, *90*, 7364–7364.
[6] F. Alonso, I. P. Beletskaya, M. Yus, *Chem. Rev.* **2004**, *104*, 3079–3160.
[7] R. J. Schwamm, M. D. Anker, M. Lein, M. P. Coles, *Angew. Chem. Int. Ed.* **2019**, *58*, 1489–1493.
[8] H. D. Patel, T. Fallon, *Org. Lett.* **2022**, *24*, 2276–2281.
[9] H. Martinez, N. Ren, M. E. Matta, M. A. Hillmyer, *Polym. Chem.* **2014**, *5*, 3507–3532.
[10] J. Greenough, Z. Zhou, Z. Wei, M. A. Petrukhina, *Dalton Trans.* **2019**, *48*, 5614–5620.
[11] K. Miyajima, T. Kurikawa, M. Hashimoto, A. Nakajima, K. Kaya, *Chem. Phys. Lett.* **1999**, *306*, 256–262.
[12] P. Lu, H. Hong, G. Cai, P. Djurovich, W. P. Weber, M. E. Thompson, *J. Am. Chem. Soc.* **2000**, *122*, 7480–7486.
[13] S. D. Houston, T. Fahrenhorst-Jones, H. Xing, B. A. Chalmers, M. L. Sykes, J. E. Stok, C. F. Soto, J. M. Burns, P. V. Bernhardt, J. J. D. Voss, G. M. Boyle, M. T. Smith, J. Tsanaktsidis, G. P. Savage, V. M. Avery, C. M. Williams, *Org. Biomol. Chem.* **2019**, *17*, 6790–6798.
[14] J. H. Noordik, T. E. M. van den Hark, J. J. Mooij, A. A. K. Klaassen, *Acta Crystallogr. Sect. B* **1974**, *30*, 833–835.
[15] N. Hu, L. Gong, Z. Jin, W. Chen, *J. Organomet. Chem.* **1988**, *352*, 61–66.
[16] R. G. Hayes, J. L. Thomas, *J. Am. Chem. Soc.* **1969**, *91*, 6876–6876.
[17] K. O. Hodgson, F. Mares, D. F. Starks, A. Streitwieser, *J. Am. Chem. Soc.* **1973**, *95*, 8650–8658.
[18] C. W. DeKock, S. R. Ely, T. E. Hopkins, M. A. Brault, *Inorg. Chem.* **1978**, *17*, 625–631.
[19] V. Lorenz, B. M. Schmiege, C. G. Hrib, J. W. Ziller, A. Edelmann, S. Blaurock, W. J. Evans, F. T. Edelmann, *J. Am. Chem. Soc.* **2011**, *133*, 1257–1259.
[20] Z. Zhou, J. McNeely, J. Greenough, Z. Wei, H. Han, M. Rouzières, A. Yu, Rogachev, R. Clérac, M. A. Petrukhina, *Chem. Sci.* **2022**, *13*, 3864–3874.
[21] L. Münzfeld, S. Gillhuber, A. Hauser, S. Lebedkin, P. Hädinger, N. D. Knöfel, C. Zovko, M. T. Gamer, F. Weigend, M. M. Kappes, P. W. Roesky, *Nature* **2023**, *620*, 92–96.
[22] W. Huber, A. M. Und, K. Müllen, *Chem. Ber.* **1981**, *114*, 1318–1336.
[23] Y. Zhu, Z. Zhou, Z. Wei, A. Tsybizova, R. Gershoni-Poranne, M. A. Petrukhina, *ChemistryEurope* **2024**, *2*, e202400055.
[24] Z. Zhou, Y. Zhu, Z. Wei, J. Bergner, C. Neiß, S. Doloczki, A. Görling, M. Kivala, M. A. Petrukhina, *Chem. Commun.* **2022**, *58*, 3206–3209.
[25] S. N. Spisak, A. V. Zabula, M. V. Ferguson, A. S. Filatov, M. A. Petrukhina, *Organometallics* **2013**, *32*, 538–543.
[26] Z. Zhou, Y. Zhu, J. M. Fernández-García, Z. Wei, I. Fernández, M. A. Petrukhina, N. Martín, *Chem. Commun.* **2022**, *58*, 5574–5577.
[27] M. Pennachio, Z. Wei, M. Mamada, M. Frigoli, M. A. Petrukhina, *Chem. Commun.* **2024**, *60*, 9526–9529.
[28] Y. Zhu, Z. Zhou, Z. Wei, M. A. Petrukhina, *J. Organomet. Chem.* **2023**, *999*, 122805.
[29] Z. Zhou, Z. Wei, Y. Tokimaru, S. Ito, K. Nozaki, M. A. Petrukhina, *Angew. Chem. Int. Ed.* **2019**, *58*, 12107–12111.
[30] N. J. Sumner, S. N. Spisak, A. S. Filatov, A. Yu, Rogachev, A. V. Zabula, M. A. Petrukhina, *Organometallics* **2014**, *33*, 2874–2878.
[31] S. N. Spisak, A. V. Zabula, A. S. Filatov, M. A. Petrukhina, *J. Organomet. Chem.* **2015**, *784*, 69–74.
[32] S. N. Spisak, Z. Zhou, S. Liu, Q. Xu, Z. Wei, K. Kato, Y. Segawa, K. Itami, A. Yu, Rogachev, M. A. Petrukhina, *Angew. Chem. Int. Ed.* **2021**, *60*, 25445–25453.
[33] S. N. Spisak, J. Li, A. Yu, Rogachev, Z. Wei, T. Amaya, T. Hirao, M. A. Petrukhina, *Organometallics* **2017**, *36*, 4961–4967.
[34] Z. Zhou, M. A. Petrukhina, *Coord. Chem. Rev.* **2023**, *486*, 215144.
[35] A. Kasprzak, *Angew. Chem. Int. Ed.* **2024**, *63*, e202318437.
[36] A. Kasprzak, M. Matczuk, H. Sakurai, *Chem. Commun.* **2023**, *59*, 9591–9594.
[37] A. Kasprzak, A. Gajda-Walczak, A. Kowalczyk, B. Wagner, A. M. Nowicka, M. Nishimoto, M. Koszytkowska-Stawińska, H. Sakurai, *J. Org. Chem.* **2023**, *88*, 4199–4208.
[38] Z. Zhou, J. M. Fernández-García, Y. Zhu, P. J. Evans, R. Rodríguez, J. Crassous, Z. Wei, I. Fernández, M. A. Petrukhina, N. Martín, *Angew. Chem. Int. Ed.* **2022**, *61*, e202115747.
[39] S. N. Spisak, J. Li, A. Yu, Rogachev, Z. Wei, O. Papaianina, K. Amsharov, A. V. Rybalchenko, A. A. Goryunkov, M. A. Petrukhina, *Organometallics* **2016**, *35*, 3105–3111.
[40] Y. Zhu, J. Borstelmann, O. Bertleff, J. Bergner, Z. Wei, C. Neiss, A. Görling, M. Kivala, M. A. Petrukhina, *J. Am. Chem. Soc.* **2024**, *146*, 14715–14723.
[41] Y. Guo, H. S. Torchon, Y. Zhu, Z. Wei, Z. Zhang, H. Han, M. A. Petrukhina, Z. Zhou, *Chem. Sci.* **2023**, *14*, 13219–13227.
[42] R. Rathore, P. Le Magueres, S. V. Lindeman, J. K. Kochi, *Angew. Chem. Int. Ed.* **2000**, *39*, 809–812.
[43] A. J. Bridgeman, G. Cavigliasso, L. R. Ireland, J. Rothery, *J. Chem. Soc. Dalton Trans.* **2001**, *14*, 2095–2108.
[44] N. V. Kozhemyakina, J. Nuss, M. Jansen, *Angew. Chem.* **2009**, *635*, 1355–1361.
[45] W. Stawski, Y. Zhu, Z. Wei, M. A. Petrukhina, H. L. Anderson, *Chem. Sci.* **2023**, *14*, 14109–14114.

Manuscript received: October 28, 2024
Revised manuscript received: December 24, 2024
Version of record online: January 15, 2025